Historical and future trends in wetting and drying in 291 catchments across China

Zhongwang Chen[1,2], Huimin Lei[1,2], Hanbo Yang[1,2], Dawen Yang[1,2], and Yongqiang Cao[3]

[1]Department of Hydraulic Engineering, Tsinghua University, Beijing, 100084, China
[2]State Key Laboratory of Hydro-Science and Engineering, Tsinghua University, Beijing, 100084, China
[3]School of urban planning and Environmental science, Liaoning Normal University, Dalian, 116029, China

Correspondence to: Hanbo Yang (yanghanbo@tsinghua.edu.cn)

Abstract

An increasingly uneven distribution of hydro-meteorological factors related to climate change has been detected by global climate models (GCMs), and the pattern of changes in water availability is commonly described with the phrase "*dry gets drier, wet gets wetter*" (DDWW). However, the DDWW pattern is dominated by oceanic areas, and recent studies based on both observed and modelled data have failed to verify the DDWW pattern on land. This study confirms the existence of a new DDWW pattern in China after analysing the observed streamflow data from 291 Chinese catchments from 1956 to 2000, revealing that the distribution of water resources has become increasingly uneven since 1950s. This pattern can be more accurately described as "*drier regions are more likely to become drier, whereas wetter regions are more likely to become wetter*". Based on a framework derived from the Budyko hypothesis, this study estimates runoff trends via observations of precipitation (P) and potential evapotranspiration (E_p) and predicts the future trends from 2001 to 2050 according to the projections of five GCMs from the Coupled Model Intercomparison Project Phase 5 (CMIP5) under three scenarios (RCP2.6, RCP4.5 and RCP8.5). The results show that this framework has a good performance for estimating runoff trends and that changes in P plays the most significant role. Most areas of China (over 60%) will experience water resource shortages under the projected climate changes. Despite the differences among the predicted results of the different models, the DDWW pattern does not hold in the projections, regardless of the model used. Nevertheless, this conclusion remains tentative due to the large uncertainties in the GCM outputs.

1 Introduction

Terrestrial water availability is critical to human lives and economic activities (Milly et al., 2005). In recent decades, changes in water availability have had significant effects on human society (Piao et al., 2010) and the environment (Arnell, 1999) in the context of climate change. Runoff (Q) is a commonly adopted indicator of water availability (Milly et al., 2005). The response of Q to climate change has been widely investigated from the basin scale to the global scale, based on streamflow

observations (e.g., Pasquini and Depetris, 2007; Dai et al., 2009; Stahl et al., 2010) or model outputs (e.g., Hamlet et al., 2007; Alkama et al., 2013; Greve et al., 2014).

Under climate change, a trend towards more uneven distribution of the hydro-meteorological elements has been detected at the global scale by the global climate models (GCMs) both spatially (Held and Soden, 2006; Chou et al., 2009) and temporally (Chou et al., 2013), as well as the observed data (Allan, 2010; Durack, 2012; Liu, 2013). This trend results in probable enhancement of hydrological extremes such as floods and droughts. This response is known as the "rich-get-richer" mechanism (Chou and Neelin, 2004), from which follow-up studies derive diverse summaries of different elements, such as "*dry gets drier, wet gets wetter*" for precipitation (P) (Allan, 2010) and precipitation minus evapotranspiration ($P-E$) (Held and Soden, 2006), "*wet season gets wetter, dry season gets drier*" for seasonal precipitation (Chou et al., 2013) and "*fresh gets fresher, salty gets saltier*" for ocean salinity (Durack, 2012; Roderick et al., 2014). Furthermore, it attracts a lot of attention to explore whether there exists a similar effect in Q on land as the "*dry gets drier, wet gets wetter*" (DDWW hereinafter for short) pattern found in $P-E$, which indicates the increasingly uneven distribution of the water resources. The original DDWW pattern predicted a simple active proportional relationship between $P-E$ and $\Delta(P-E)$, as the sign of $P-E$ determines whether a region is dry (negative) or wet (positive). It should be noticed that the predicted changes were averages of latitudinal zones rather than values at the local scale (e.g., grid box or catchment), resulting in the dominance of the oceanic components in the DDWW pattern (Roderick et al., 2014), as P and E are dominated by exchanges over the ocean at most latitudes (Lim and Roderick, 2009). Thus, the DDWW pattern is more appropriately applied to the ocean than to the land. In fact, because the long-term mean $P-E$ is overwhelmingly positive on land, the method of using the sign of $P-E$ to identify wet and dry regions is not feasible anymore, as $\Delta(P-E)$ can obviously be negative. Therefore, some scholars tried to explore a new DDWW pattern to describe changes in the hydrological cycle on land at the local scale. Greve et al. (2014) adopted the aridity index (φ, $=E_p/P$, where E_p denotes the potential evapotranspiration) as a measurement of the aridity degree, and defined $\varphi>2$ as dry regions and $\varphi<2$ as wet regions. Consequently, the pattern became "$\varphi>2$, $\Delta(P-E)<0$; whereas $\varphi<2$, $\Delta(P-E)>0$". However, the results, based on more than 300 combinations of various global hydrologic data sets containing both observed and modelled data, showed that only 10.8% of land areas robustly followed the adjusted DDWW pattern. Nevertheless, the study of Greve et al. (2014) still has some defects related to two major aspects: one is the existence of large uncertainties in E in both the satellite-based observations and the simulations (Kumar et al., 2016), and the other is artificially assigned threshold between the wet and dry regions, which, when the threshold is changed, changes the results. Therefore, a study based on observed Q data that are more direct and of relatively low uncertainty should be conducted as well as a new method to partition dry and wet regions not depending on the appointed threshold.

However, it should be noted that the observed changes in Q are not only responses to climate change but are also responses to other factors, such as land cover changes and human activities, e.g., withdrawal and drainage (Stahl et al., 2010). To extract the components related only to climate change is an intractable process because there is no effective method to do so. Therefore, a roundabout means is to compare the credibly estimated changes in Q under the influence of climate change

with those of the observed data. The Budyko hypothesis (Budyko, 1948) is a robust and simple tool that can accurately model mean annual Q within a catchment based only on meteorological information under climate change (Koster and Suarez, 1999). The Budyko hypothesis depicts the long-term coupled water-energy balance for a catchment as

$$\overline{E}/\overline{P} = f(\overline{E_p}/\overline{P}, c), \quad (1)$$

where the function f denotes Budyko-like equations, $\overline{E_p}$ is the mean annual potential evapotranspiration, and c is a parameter characterizing a particular catchment. There are various types of Budyko-like equations (e.g., Pike, 1964; Fu, 1981; Choudhury, 1999; Zhang et al., 2001; Yang et al., 2008; Wang and Tang, 2014; Zhou et al., 2015). The Budyko hypothesis has been examined and applied in both observation-based (Zhang et al., 2001; Oudin et al., 2008; Xu et al., 2014) and model-based studies (Zhang et al., 2008; Teng et al., 2012) and produces good consistency between observed and modelled data. By analysing hydro-meteorological data from 108 nonhumid catchments in China, Yang et al. (2007) confirmed that the Budyko hypothesis is capable of predicting Q both at long-term and annual time scales. Xiong and Guo (2012) assessed the Budyko hypothesis in 29 humid watersheds in southern China and found that parametric Budyko formulae can estimate the long-term average Q well. Therefore, it is reasonable to estimate Q using the Budyko hypothesis in China. The ability of the Budyko hypothesis to capture the effects of climate change on Q, as well as other details, is described in Section 2.3.

Based on observed streamflow data from 291 catchments in China, this study first analyses the historical trends in annual Q, to explore the possible existence of a DDWW pattern via a new method proposed in Section 2.2. Then, adopting a simple framework derived from the Budyko hypothesis stated in Section 2.3, this study estimates the runoff trends caused by climate change in the study catchments, to reveal that the historical trends are mainly a response to climate change and identify the key influencing factor. Moreover, based on the Coupled Model Intercomparison Project Phase 5 (CMIP5) projections of five GCMs, this study predicts changes in Q via the framework to determine whether the DDWW pattern will continue to hold in the future.

2 Data and methods

2.1 Study area and data

This study collected hydrologic and meteorological data from 291 catchments in mainland China with drainage areas ranging from 372 to 142,963 km^2. These catchments cover all the first-level basins of mainland China except the Huaihe River Basin (**Figure 1)**. Annual restored discharge data from 1956 to 2000 for each catchment outlet were collected from the Hydrological Bureau of the Ministry of Water Resources of China. Here, the "restored" means that the effects of human activities on discharge have been mostly removed via the water balance method or other methods. Specifically, the process of restoring the station-observed discharge consists of two major parts: replenishing the consumption and removing the introduction. The water consumption includes the net consumption in agricultural, industrial and residential sectors as well as water loss in the reservoir due to evaporation and leakage. The introduction part includes the water diverted from other

watersheds and the extracted groundwater back into the river. The change in the reservoir storage can be either part depending on whether the change is positive or negative. Thus, the restored discharge can be considered the natural discharge (or very close). The records range in length from 21 years to 45 years, and 261 catchments have record lengths greater than 40 years.

Two meteorological data sets were used in this study. One is the 10 km gridded data set interpolated by Yang et al. (2014) based on 736 stations of the China Meteorological Administration, including P and potential evapotranspiration (E_p) observations from 1956 to 2000. Based on this observed data set, the annual areal P and E_p of each catchment were calculated. The other is the daily bias-corrected (see Piani et al., 2010 and Hagemann et al., 2011) modelled data set from the Inter-Sectoral Impact Model Intercomparison Project (ISI-MIP, http://www.isi-mip.org) covering the period 1951–2050 under scenarios RCP2.6, RCP4.5 and RCP8.5, as released by the CMIP5. These modelled data were initially downscaled to a 0.5°×0.5° latitude–longitude grid then extracted and transformed into the ASCII format by the Institute of Environment and Sustainable Development in Agriculture, the Chinese Academy of Agricultural Sciences, China. The output data for each scenario include precipitation; mean, maximum and minimum air temperature; solar radiation; wind speed; and relative humidity for the five models (GFDL-ESM2M, HadGEM2-ES, IPSL-CM5A-LR, MIROC-ESM-CHEM and NorESM1-M). The daily E_p was estimated for each grid by the Penman Equation (Penman, 1948; see Appendix A for more details) based on the GCM outputs. Annual series of P and E_p were calculated as the sum of every daily P and E_p over a year. Then, annual catchment-averaged P and E_p data was calculated as the average of grid P and E_p within one catchment.

2.2 Runoff trends and the DDWW pattern

In this study, to estimate runoff trend, we used two slightly different methods for the historical (1956-2000) and projected period (2001-2050), respectively. The runoff trend for the historical period was estimated as the slope of the linear regression of the annual Q series, denoted by k_Q, and can be calculated by

$$k_Q=\frac{\sum_{i=1}^{m}(t_i-\bar{t})(Q_i-\bar{Q})}{\sum_{i=1}^{m}(t_i-\bar{t})^2}, \quad (2)$$

where m is the observed record length of a catchment, i is the ith record, t_i is the year of this record, $\bar{t}$ is the average of all record years, as Q_i and $\overline{Q}$ are the observed annual runoff in t_i and the mean annual runoff in historical period, respectively. The significance of k_Q was tested using a t-test. The runoff trend of the projected period was denoted as $\Delta\overline{Q}$, defined as the change in mean annual runoff between historical and projected period, and can be computed as follows:

$$\Delta\overline{Q}=\overline{Q}_p-\overline{Q}, \quad (3)$$

where $\overline{Q}_p$ denotes the projected mean annual runoff.

In the study of Greve et al. (2014), the DDWW pattern was sensitive to the assigned threshold for defining the dry and wet regions, i.e., different thresholds may lead to different (possibly conflicting) results. To remove the influence of the threshold, Allan et al. (2010) adopted percentile bins for P to define wet and dry regions, thereby successfully avoiding the pitfalls of

selecting a convincing threshold. Therefore, this study does not define absolute "wet" or "dry" regions but instead identifies relative "wetter" or "drier" ones. To be specific, two variables were chosen to be the indicators of the aridity index, $\overline{Q}$ and φ, respectively. The term φ is introduced to maintain consistency with studies based on the climate model data where $\overline{Q}$ is not available. The spatial distribution of $\overline{Q}$ and φ are shown in **Figure 2**, with $\overline{Q}$ ranging from 0 to 1400 mm a^{-1} and φ ranging from 0.5 to 8. We divide $\overline{Q}$ and φ into six intervals, the intervals with larger $\overline{Q}$ values and smaller φ values are wetter levels (**Table 1**). In each interval, the total catchments and becoming wetter catchments were counted, and then the proportion of wetter catchments, denoted as d, was calculated. A larger d value implies that more catchments have become wetter in this level. This study compares the d values of different intervals to examine a new DDWW pattern.

2.3 A framework to estimate runoff trends under climate change

Among various types of Budyko-like equations, two analytical equations proposed by Fu (1981) and Yang et al. (2008) should be highlighted. Because these two studies each introduce a catchment property parameter, ω and n, respectively (two examples of c in Equation (1)), the two equations are able to better capture the role of landscape characteristics. Yang et al. (2008) showed a high linear correlation between ω and n. Therefore, this study chooses the equation derived by Yang et al. (2008), which has been rewritten as follows:

$$\frac{\overline{E}}{\overline{P}} = \left[\left(\frac{\overline{E_{\mathrm{p}}}}{\overline{P}}\right)^{-n} + 1\right]^{-1/n}. \tag{4}$$

Focusing on Q, this study transforms Equation (4) into

$$\overline{Q} = \overline{P} - \overline{P}\left[\left(\frac{\overline{E_{\mathrm{p}}}}{\overline{P}}\right)^{-n} + 1\right]^{-1/n}. \tag{5}$$

The parameter n can be calculated using the observed $\overline{Q}$, $\overline{P}$ and $\overline{E_{\mathrm{p}}}$ of each catchment from the period of 1956 to 2000. The differential form of Equation (5) is derived as follows:

$$dQ = \frac{\partial Q}{\partial P}dP + \frac{\partial Q}{\partial E_{\mathrm{p}}}dE_{\mathrm{p}} + \frac{\partial Q}{\partial n}dn, \tag{6}$$

where dQ, dP, dE_{p} and dn denote deviations in the observed or modelled Q, P, E_{p} and n with respect to long-term mean value. Equation (6) has widely been used to estimate changes in annual Q (e.g., Yang and Yang, 2011; Roderick and Farquhar, 2011; Roderick et al., 2014).

Since we focus on the effects of climate change, n is assumed to remain unchanged, i.e., dn equalling 0 (Yang and Yang, 2011), and Equation (6) becomes

$$dQ = \frac{\partial Q}{\partial P}dP + \frac{\partial Q}{\partial E_{\mathrm{p}}}dE_{\mathrm{p}}. \tag{7}$$

For convenience, we introduce ε_P and ε_0 to represent $\frac{\partial Q}{\partial P}$ and $\frac{\partial Q}{\partial E_{\mathrm{p}}}$, which can be estimated based on n, $\overline{P}$ and $\overline{E_{\mathrm{p}}}$:

$$\varepsilon_P=\left.\frac{\partial Q}{\partial P}\right|_{(\overline{P},\overline{E_p})}=1-\left[1+\left(\frac{\overline{E_p}}{\overline{P}}\right)^{-n}\right]^{\frac{n+1}{n}} \text{ and}$$

$$\varepsilon_0=\left.\frac{\partial Q}{\partial E_p}\right|_{(\overline{P},\overline{E_p})}=-\left[1+\left(\frac{\overline{E_p}}{\overline{P}}\right)^{n}\right]^{\frac{n+1}{n}}.$$

Roderick et al. (2014) showed that the runoff changes (=$\Delta(P-E)$ in this study) estimated using Equation (7) account for around 82% of the variation in the GCM projections of $\Delta(P-E)$. Therefore, Equation (7) can predict a reliable result under climate change projected by GCMs. Based on Equation (7), a framework can then be constructed to estimate runoff trends (see Appendix B for interpretation):

$$k_{Qe}=\varepsilon_P k_P+\varepsilon_0 k_{E_p}, \quad (8a)$$

$$\Delta\overline{Q}_e=\varepsilon_P\Delta\overline{P}+\varepsilon_0\Delta\overline{E_p}, \quad (8b)$$

where k_{Qe} and $\Delta\overline{Q}_e$ are estimated runoff trends of the historical and projected period, respectively; k_P and k_{E_p} are the linear regression-calculated trends in annual P and E_p, respectively; and $\Delta\overline{P}$ and $\Delta\overline{E_p}$ are changes in $\overline{P}$ and $\overline{E_p}$, respectively.

Equations (8a) and (8b) attribute the runoff trend to two major factors, the precipitation trend and the potential evapotranspiration trend. Equation (8a) estimates k_{Qe} according to the observed k_P and k_{E_p}. Equation (8b) estimates $\Delta\overline{Q}_e$ according to the GCM projections, and $\Delta\overline{P}$ and $\Delta\overline{E_p}$ are calculated as differences in $\overline{P}$ and $\overline{E_p}$ between 1956–2000 and 2001–2050. Due to the uncertainty of the GCMs, the coefficient of variance (C_v) in each catchment is estimated. The C_v is defined as the ratio between the standard deviation and the absolute mean of the five $\Delta\overline{Q}_e$ outputs of the respective GCMs. Specifically, a lower C_v indicates less uncertainty in $\Delta\overline{Q}_e$ because the results of the different GCMs are similar.

3 Results

3.1 Historical trends in annual runoff

Figure 3 presents the spatial distribution of observed k_Q in the 291 study catchments. At the significance level of 0.05, 39.9% (116 of 291) of the study catchments are undergoing significant changes in annual Q and are called "significant catchments" in the following text. Trends towards wetter conditions (positive trends) are found mainly in the upper and lower reaches of the Yangtze River basin, the Southwest and the Southeast Rivers basin, the Pearl River basin and the Inland Rivers basin. The annual Q in the lower reaches of the Yangtze River basin and the Northern Xinjiang Uygur Autonomous Region is robustly increasing by over 2 mm a^{-1}, which is greater than the rates of most other catchments. The largest increasing trend of 10.3 mm a^{-1} is observed in the Yangtze River basin. However, the catchments in the middle reaches of the Yangtze River basin and in northern and northeastern China are experiencing the greatest reductions in runoff, generally with significant

trends. Several catchments have negative trends of over 4 mm a^{-1}, and the most severe situation is in the Yellow River basin, where the annual Q is decreasing at a rate of 7.2 mm a^{-1}.

The relationship between k_Q and $\overline{Q}$ is plotted in **Figure 4**, which also shows the d for each interval. With increasing $\overline{Q}$, d increases from 0.18 to 0.88, which means that "*drier regions are more likely to become drier, whereas wetter regions are more likely to become wetter*". The slight decrease in d to 0.79 in the last interval can be attributed to the small sample size of this interval, as the number of catchments getting drier is actually equal in intervals 5 and 6 (**Table 2**). Therefore, it indicates a new DDWW pattern. This pattern emphasizes the fact that the distribution of water resources has become more uneven in China since 1950s. The process driving the uneven distribution of water resources in this study is powerful because nearly all the wettest catchments became wetter and the driest catchments became drier.

Moreover, the DDWW pattern was explored based on k_Q and φ is when $\overline{Q}$ is not available. **Figure 5** shows that d decreases from 0.86 to 0.16 as φ increases, implying that the DDWW pattern also holds if we adopt φ to describe the aridity degree, similar to Greve et al. (2014). It is because of the monotonic decrease in $\overline{Q}$ with φ (**Figure 6a**). However, d increases sharply to 0.36 in the last interval, in contrast to the DDWW pattern. To understand this divergence, we have marked areas with $\varphi > 2$ and $k_Q > 0$ (26 in total) in **Figure 6b**. Surprisingly, most of these areas (19 of 26) are located in areas with glaciers. Therefore, the changes in water storage (ΔS) from the melting of glacial ice and snow also play a key role in the runoff generation there. However, φ does not consider the influence of ΔS, thereby leading to an overestimation of the aridity degree in these catchments, i.e., they are grouped into the wrong intervals. This reflects the weakness of the ability of φ to assess the aridity degree with respect to water resources compared to $\overline{Q}$. Moreover, if acquiring $\Delta S$and redefining an adjustable aridity index (φ') as $(P - \Delta S)/E_p$, it is possible that these catchments with high φ also obey the DDWW pattern.

3.2 Interpreting the trends from climate change perspective

Based on a comparison of the Budyko-estimated k_{Qe} with observed k_Q, the coefficients of determination (R^2) (Legates and McCabe, 1999) are 0.70 and 0.86 for all catchments and for significant catchments, respectively (**Figure 7**).Therefore, the majority of the runoff trends can be attributed to changes in the atmospheric forcing of water and energy. However, the slope k is smaller than one (0.60 and 0.62 for all catchments and significant catchments, respectively), implying that the Budyko-based framework underestimates the changes in runoff. Nevertheless, despite underestimating the runoff trends, the framework can correctly note the direction of runoff changes in more than 80% of the study catchments (**Figure 7**), as the error rates (proportions of misestimated catchments that have different signs of observed and estimated trends) in all and significant catchments are 18.6% (54 of 291) and 6.0% (7 of 116), respectively. Furthermore, the DDWW pattern works well based on k_{Qe} (**Figure 8**), which validates the DDWW pattern from the perspective of climate change based on historical meteorological observations. It also indicates the feasibility of using only P and E_p information to examine the pattern, and serves as a reference for studies based on climate model outputs.

In catchments where the observed and estimated signs are consistent, the parts of k_{Qe} generated from P (k_Q^P, $=\varepsilon_P k_P$) and E_p (k_Q^0, $=\varepsilon_0 k_{E_p}$) are compared to find the factor controlling the runoff changes due to climate change. As shown in **Figure 9**, k_P makes an overwhelming contribution in 88.6% (210 of 237) of these catchments, as ratios of absolute k_Q^0 to absolute k_Q^P are smaller than 1. Moreover, when linking k_P with $\overline{Q}$ (**Figure 10**), we observe a pattern similar to the DDWW pattern, i.e., "more precipitation in wetter areas, and less in drier areas". This pattern is the result of the dominant position of k_P and the positive effect of k_P on the runoff trends. Therefore, from the perspective of climate change, the more uneven precipitation results in more uneven runoff, producing the DDWW pattern.

3.3 Predicting future trends using the GCM projections

Based on the GCM projections, equation (8b) predicts the future runoff trends $\Delta\overline{Q}_e$ between the periods of 1956–2000 and 2001–2050. The results show that great discrepancies appear in $\Delta\overline{Q}_e$ among the five GCMs even under the same scenario, whereas the model-averaged results under different scenarios are close (**Figure 11**). The C_v values of $\Delta\overline{Q}_e$ in each catchment are presented in **Figure 12**. Taking the RCP2.6 scenario as an example, over two-fifths (41.9%) of the catchments have a C_v value larger than 0.5, which is indicative of considerable uncertainty in the various models reported by previous studies (e.g., Greve et al., 2014; Kumar et al., 2016). However, the proposed DDWW pattern is no longer suitable under the three scenarios, regardless of which model is selected, because d decreases as $\overline{Q}$ increases, except for an increase in interval 6, in contrast to the DDWW pattern. However, it doesn't mean an obvious alleviation of the uneven water resource distribution but conveys a bad news that most areas of China (over 60%, calculated from **Table 3**) will experience water resource shortages under the projected climate changes, whereas the changes in the conditions of the driest (interval 6) and wettest (interval 1) areas are relatively slight. Furthermore, the main meteorological factor controlling the future trends was identified based on the mean values of the five GCMs. **Figure 13** shows that trends in P ($\Delta\overline{P}$) are no longer the controlling factor, as only 40% of the catchments have values of $\left|\frac{\varepsilon_0\Delta\overline{E_p}}{\varepsilon_P\Delta\overline{P}}\right|$ smaller than 1.

The spatial distribution of model-averaged relative changes in $\overline{Q}$ ($\Delta\overline{Q}_e/\overline{Q}$) is shown in **Figure 14**. The results under the three scenarios are similar. Red regions are catchments where $\overline{Q}$ will fall by more than 60% relative to the historical value, and most of these regions are located in the Yellow River Basin with relatively high certainty (C_v<0.5). The most severe situation arises in a catchment situated in the Yangtze River Basin, where the runoff is predicted to be nearly zero and the C_v is less than 0.2. In contrast, dark blue areas are catchments where $\overline{Q}$ is projected to increase by over 40%. These catchments are primarily located in the Inland River Basin, except for Northwest China, where catchments will suffer from a shortage of fresh water. Instead of continuing to become drier, catchments in Northeast and North China are projected to generate more runoff in the future, whereas catchments in the lower reaches of the Yangtze River Basin will experience considerable

reductions in runoff, despite historical increases. These are the most obvious distinctions between the projected and historical runoff changes. Thus, the DDWW pattern fails to accurately characterize these future patterns.

However, an inevitable concern about the GCM outputs is their uncertainty, which determines the reliability of the projected results. To examine the uncertainty, one workable method is to compare meteorological observations with simulations for the period of 1956–2000. Taking the results of the GFDL-ESM2M model as an example (**Figure 15**), $\overline{P}$ is simulated well except for some obvious incorrectly estimated points far from the $y = x$ line. However, simulations of $\overline{E_p}$ show tremendous deviations, resulting in no obvious linear relationship between the simulated and observed values. This simple comparison directly highlights the unreliability of the GCM outputs.

4 Discussion

In the present work, a new method not limited to the artificial selection of the threshold to partition dry and wet regions is proposed to examine the DDWW pattern. Our results confirmed that a feasible DDWW pattern exists in the historical runoff trends across China. However, if we adopted the same threshold φ=2 as Greve et al. (2014) to check **Figure 5**, we would get the totally opposite result that the DDWW pattern doesn't hold. Therefore, the use of the new method may also verify the validity of the DDWW pattern in previous studies. Roderick et al., (2014) plotted the relationship between GCM-based gridded $\Delta(P - E)$ and $P - E$ over land (Fig.1.(f) in the study of Roderick et al., (2014)) to argue that the proportional relationship between them revealed by Held and Soden (2006) doesn't hold over land anymore. Nevertheless, seen from the new method's perspective, the relationship seems consistent with the DDWW pattern found in this study, that the possibility of $\Delta(P - E)>0$ gets larger as $P - E$ gets larger. Additionally, the DDWW pattern might also hold in the study of Greve et al. (2014) according to Figure 4c in that study and the distribution of φ across the world. Therefore, a follow-up to this study is to promote the proposed method to the worldwide scale, to examine the DDWW pattern globally.

Based on a Budyko-based framework, our findings suggest that climate change is the main reason resulting in the historical runoff trends and k_P is the most significant factor associated with climate change. Roderick et al. (2014) reported a similar result in their research of GCM outputs (CMIP3), that the changes in water availability ($\Delta(P - E)$) are dominated by the changes in P (ΔP) globally. Despite high correlation between k_Q and k_{Qe}, the Budyko-based framework underestimates the observed changes in runoff. This is because the framework only quantifies the effects of climate change, and the estimated deviation may stem from the neglect of other influencing factors, such as ecological and environmental changes, that result in changes in the catchment properties (dn in Equation 6) that we assume to be constant in this study.

In this study, E_p was calculated using the Penman Equation, which is considered one of the best way (Zhang et al., 2001) and is strongly recommended by Shuttleworth (2012). This method to estimate E_p is also adopted by other studies, e.g., Yang et al., (2014) and Xu et al. (2015) However, Roderick et al., (2015) suggested using the net radiation instead of E_p in the

Budyko hypothesis. Kumar et al., (2016) compared runoff change projections obtained by these two different methods, finding a similar result. Therefore, it is likely that the use of E_p or net radiation has little influence in our results.

Our results showed that great discrepancy arises between the GCM-simulated and observed $\overline{E_p}$, whereas GCM-simulated and observed $\overline{P}$ are way more coincident (**Figure 15**). This tremendous distinction in GCM's performance in $\overline{P}$ and $\overline{E_p}$ simulations evokes doubts about the reliability of the bias-corrected GCM outputs used in this study. Actually, the bias-correction process had been implemented to all GCM outputs, meaning all variables needed to calculate E_p were corrected simultaneously. We speculate that it might relate to the disparate effectiveness of the bias-correction process in different outputs, resulting in good fit to P and bad fit to E_p.

5 Conclusions

Based on the analysis of restored discharge in 291 catchments across China from 1956 to 2000, we proposed a suitable DDWW pattern that "*drier regions are more likely to become drier, whereas wetter regions are more likely to become wetter*", which implies that the distribution of the water resources in China has become more uneven since the 1950s. The pattern holds both in the studies adopting $\overline{Q}$ and φ as the indicator of water availability. Furthermore, a framework based on the Budyko hypothesis reveals that the runoff changes can be mainly attributed to climate change and k_P is the controlling factor. According to the projections of five GCMs from CMIP5 during the period of 2001-2050, the proposed DDWW pattern is no longer suitable. The model-average results suggest that over 60% of catchments will experience water resource shortages under future climate change. In addition, only 40% of the study catchments will be primarily controlled by $\Delta\overline{P}$, which is different from the phenomenon that the runoff change was controlled by precipitation in about 90% catchments in the historical period. The catchments in Northeast and North China, which were becoming drier, will generate more runoff in the future, whereas the catchments in the lower reaches of the Yangtze River Basin, which were becoming wetter, will experience considerable reductions in runoff. These changes represent the most obvious differences between the projected and historical runoff changes. Nevertheless, the projected conclusions remain tentative due to the enormous unreliability of the GCM outputs as indicated by the extremely low correlations between the simulated and observed $\overline{E_p}$ values for the period of 1956–2000.

The results of this study may serve as a helpful case to explore the rule of spatial heterogeneity in runoff trends and to supplement the study of the DDWW pattern under climate change. Though some studies suspected the existence of the DDWW pattern in land, this study proves that the DDWW pattern actually exists across China in history. It is essential to realize the more uneven distribution of water resources across China for China to better cope with climate change, as well as rationally manage and utilize water resources. Moreover, the proposed method, which divides catchments into several intervals representing different aridity degrees instead of assigning a threshold to partition wet and dry regions, can be easily promoted to the global study of the DDWW pattern and draw a more generalized conclusion over world.

Acknowledgements

This research was partially supported by funding from the National Natural Science Foundation of China (Grant Nos. 51622903 and 51379098), the National Program for Support of Top-notch Young Professionals, and the Program from the State Key Laboratory of Hydro-Science and Engineering of China (Grant Nos. sklhse-2016-A -02 and 2017-KY-01).

5

References

Alkama, R., Marchand, L., Ribes, A., and Decharme, B.: Detection of global runoff changes: results from observations and CMIP5 experiments, Hydrol. Earth Syst. Sci., 17, 2967-2979, doi:10.5194/hess-17-2967-2013, 2013.

Allan, R. P., Soden, B. J., John, V. O., Ingram, W., and Good, P.: Current changes in tropical precipitation, Envirom. Res. Lett., 5,doi:, 10.1088/1748-9326/5/2/025205, 2010.

Arnell, N. W.: Climate change and global water resources, Glob. Environ. Change, 9, S31-S49, 1999.

Budyko, M. I.: Evaporation under Natural Conditions, Israel Program for Scientific Translations, Jerusalem, 1948.

Chou, C., and Neelin, J. D.: Mechanisms of global warming impacts on regional tropical precipitation, J. Climate, 17, 2688-2701,doi:, 10.1175/1520-0442(2004)017<2688:MOGWIO>2.0.CO;2, 2004.

Chou, C., Neelin, J. D., Chen, C., and Tu, J.: Evaluating the "Rich-Get-Richer" Mechanism in Tropical Precipitation Change under Global Warming, J. Climate, 22, 1982-2005,doi:, 10.1175/2008JCLI2471.1, 2009.

Chou, C., Chiang, J. C. H., Lan, C., Chung, C., Liao, Y., and Lee, C.: Increase in the range between wet and dry season precipitation, Nat. Geosci., 6, 263-267, doi:10.1038/ngeo1744, 2013.

Choudhury, B. J.: Evaluation of an empirical equation for annual evaporation using field observations and results from a biophysical model, J. Hydrol., 216, 99-110, doi:10.1016/S0022-1694(98)00293-5, 1999.

Dai, A., Qian, T., Trenberth, K. E., and Milliman, J. D.: Changes in continental freshwater discharge from 1948 to 2004, J. Climate, 22, 2773-2792, doi:10.1175/2008JCLI2592.1, 2009.

Durack, P. J., Wijffels, S. E., and Matear, R. J.: Ocean Salinities Reveal Strong Global Water Cycle Intensification During 1950 to 2000, Science, 336, 455-458,doi:, 10.1126/science.1212222, 2012.

Fu, B.: On the calculation of the evaporation from land surface, Scienta Atmos. Sinica, 5, 23–31, 1981.

Greve, P., Orlowsky, B., Mueller, B., Sheffield, J., Reichstein, M., and Seneviratne, S. I.: Global assessment of trends in wetting and drying over land, Nat. Geosci., 7, 716-721, doi:10.1038/ngeo2247, 2014.

Guo, W., Liu, S., Yao, X., Xu, J., Shangguan, D., Wu, L., Zhao, J., Liu, Q., Jiang, Z., Wei, J., Bao, W., Yu, P., Ding, L., Li, G., Li, P., Ge, C. and Wang, Y.: The second glacier inventory dataset of China (Version 1.0). Cold and Arid Regions Science Data Center at Lanzhou, doi:10.3972/glacier.001.2013.db, 2014.

Hagemann, S., Chen, C., Haerter, J. O., Heinke, J., Gerten, D., and Piani, C.: Impact of a statistical bias correction on the projected hydrological changes obtained from three GCMs and two hydrology models, J. Hydrometeorol, 12, 556–578, 2011.

Hamlet, A. F., Mote, P. W., Clark, M. P., and Lettenmaier, D. P.: Twentieth-century trends in runoff, evapotranspiration, and soil moisture in the Western United States, J. Climate, 20, 1468–1486, doi:10.1175/JCLI4051.1, 2007.

Held, I. M. and Soden, B. J.: Robust responses of the hydrological cycle to global warming, J. Climate, 19, 5686-5699, doi:10.1175/JCLI3990.1, 2006.

Koster, R. D. and Suarez, M. J.: A simple framework for examining the interannual variability of land surface moisture fluxes, J. Climate, 12, 1911–1917, doi:10.1175/1520-0442(1999)012<1911:ASFFET>2.0.CO;2, 1999.

Kumar, S., Zwiers, F., Dirmeyer, P. A., Lawrence, D. M., Shrestha, R., and Werner, A. T.: Terrestrial contribution to the heterogeneity in hydrological changes under global warming, Water Resour. Res., 52, 3127-3142, doi:10.1002/2016WR018607, 2016.

Legates, D. R. and McCabe, G. J.: Evaluating the use of "goodness-of-fit" measures in hydrologic and hydroclimatic model validation, Water Resour. Res., 35, 233-241, doi:10.1029/1998WR900018, 1999.

Lim, W. H. and Roderick, M. L.: An atlas of the global water cycle: based on the IPCC AR4 Models, Australian National University Press, Canberra, 2009.

Liu, C., and Allan, R. P.: Observed and simulated precipitation responses in wet and dry regions 1850-2100, Environ. Res. Lett., 8,doi:, 10.1088/1748-9326/8/3/034002, 2013.

Milly, P. C. D., Dunne, K. A., and Vecchia, A. V.: Global pattern of trends in streamflow and water availability in a changing climate, Nature, 438, 347-350, doi:10.1038/nature04312, 2005.

Oudin, L., Andréassian, V., Lerat, J., and Michel, C.: Has land cover a significant impact on mean annual streamflow? An international assessment using 1508 catchments, J. Hydrol., 357, 303-316, doi:10.1016/j.jhydrol.2008.05.021, 2008.

Pasquini, A. I. and Depetris, P. J.: Discharge trends and flow dynamics of South American rivers draining the southern Atlantic seaboard: an overview, J. Hydrol., 333, 385-399, doi:10.1016/j.jhydrol.2006.09.005, 2007.

Penman, H. L.: Natural evaporation from open water, bare soil and grass, Proc. Royal Soc. A Math. Phys. Eng. Sci., 193, 120–145, doi:10.1098/rspa.1948.0037, 1948.

Piani, C., Weedon, G. P., Best, M., Gomes, S. M., Viterbo, P., Hagemann, S., and Haerter, J. O.: Statistical bias correction of global simulated daily precipitation and temperature for the application of hydrological models, J. Hydrol., 395, 199–215, 2010.

Piao, S., Ciais, P., Huang, Y., Shen, Z., Peng, S., Li, J., Zhou, L., Liu, H., Ma, Y., Ding, Y., Friedlingstein, P., Liu, C., Tan, K., Yu, Y., Zhang, T., and Fang, J.: The impacts of climate change on water resources and agriculture in China, Nature, 467, 43-51, doi:10.1038/nature09364, 2010.

Pike, J. G.: The estimation of annual run-off from meteorological data in a tropical climate, J. Hydrol., 2, 116-123, 1964.

Roderick, M. L., Farquhar, G. D.: A simple framework for relating variations in runoff to variations in climatic conditions and catchment properties, Water Resour. Res., 47, doi:10.1029/2010WR009826, 2011.

Roderick, M. L., Sun, F., Lim, W. H., and Farquhar, G. D.: A general framework for understanding the response of the water cycle to global warming over land and ocean, Hydrol. Earth Syst. Sci., 18, 1575–1589, doi:10.5194/hess-18-1575-2014, 2014.

Roderick, M. L., Greve, P., and Farquhar, G. D.: On the assessment of aridity with changes in atmospheric CO2, Water Resour. Res., 51, 5450-5463, doi: 10.1002/2015WR017031, 2015.

Stahl, K., Hisdal, H., Hannaford, J., Tallaksen, L. M., van Lanen, H. A. J., Sauquet, E., Demuth, S., Fendekova, M., and Jódar, J.: Streamflow trends in Europe: evidence from a dataset of near-natural catchments, Hydrol. Earth Syst. Sci., 14, 2367-2382, doi:10.5194/hess-14-2367-2010, 2010.

Shuttleworth, W. J.: Daily estimates of evaporation, in Terrestrial Hydrometeorology, 334–358, John Wiley, Chichester, U. K., doi:10.1002/9781119951933, 2012.

Teng, J., Chiew, F. H. S., Vaze, J., Marvanek, S., and Kirono, D. G. C.: Estimation of climate change impact on mean annual runoff across continental Australia using Budyko and Fu equations and hydrological models, J. Hydrometeor, 13, 1094-1106, doi:10.1175/JHM-D-11-097.1, 2012.

Wang, D. and Tang, Y.: A one-parameter Budyko model for water balance captures emergent behavior in Darwinian hydrologic models, Geophys. Res. Lett., 41, 4569-4577, 2014.

Xiong, L. and Guo, S.: Appraisal of Budyko formula in calculating long-term water balance in humid watersheds of southern China, Hydrol. Process., 26, 1370–1378, doi:10.1002/hyp.8273, 2012.

Xu, K., Yang, D., Yang, H., Li, Z., Qin, Y., and Shen, Y.: Spatio-temporal variation of drought in China during 1961-2012: A climatic perspective, J. Hydrol., 526, 253-264, doi: 10.1016/j.jhydrol.2014.09.047, 2015.

Xu, X., Yang, D., Yang, H., and Lei, H.: Attribution analysis based on the Budyko hypothesis for detecting the dominant cause of runoff decline in Haihe basin, J. Hydrol., 510, 530-540, doi:10.1016/j.jhydrol.2013.12.052, 2014.

Yang, D., Sun, F., Liu, Z., Cong, Z., Ni, G., and Lei, Z.: Analyzing spatial and temporal variability of annual water-energy balance in nonhumid regions of China using the Budyko hypothesis, Water Resour. Res., 43, doi:10.1029/2006WR005224, 2007.

Yang, H., Yang, D., Lei, Z., and Sun, F.: New analytical derivation of the mean annual water-energy balance equation, Water Resour. Res., 44, doi:10.1029/2007WR006135, 2008.

Yang, H., Yang, D.: Derivation of climate elasticity of runoff to assess the effects of climate change on annual runoff, Water Resour. Res., 47, doi:10.1029/2010WR009287, 2011.

Yang, H., Qi, J., Xu, X., Yang, D., and Lv, H.: The regional variation in climate elasticity and climate contribution to runoff across China, J. Hydrol., 517, 607-616, doi:10.1016/j.jhydrol.2014.05.062, 2014.

Zhang, L., Dawes, W. R., and Walker, G. R.: Response of mean annual evapotranspiration to vegetation changes at catchment scale, Water Resour. Res., 37, 701-708, doi:10.1029/2000WR900325, 2001.

Zhang, L., Potter, N., Hickel, K., Zhang, Y., and Shao, Q.: Water balance modeling over variable time scales based on the Budyko framework – model development and testing, J. Hydrol., 360, 117-131, doi:10.1016/j.jhydrol.2008.07.021, 2008.

Zhou, S., Yu, B., Huang, Y., and Wang, G.: The complementary relationship and generation of the Budyko functions, Geophys. Res. Lett., 42, 1781-1790, 2015.

Appendix A

The procedure for using the Penman Equation to estimate E_p (mm d^{-1}) based on the GCM outputs is described in detail in this appendix. The Penman Equation can be written as (Yang et al., 2011)

$$E_p=\frac{0.408\Delta(R_n-G)+2.624\gamma(1+0.536u_2)(1-\mathrm{RH})e_s}{\Delta+\gamma}, \quad (A.1)$$

where e_s is the saturated vapor pressure (kPa), Δ is the slope of the saturated vapour pressure versus air temperature curve (kPa °C^{-1}) when the saturated vapour pressure equals e_s, R_n is the net radiation (MJ m^{-2} d^{-1}), G is the soil heat flux (MJ m^{-2} d^{-1}), γ is a psychometric constant (kPa °C^{-1}), u_2 is the wind speed at a height of 2 m (m s^{-1}), and RH is the relative humidity (%) (Yang et al., 2011).

The form of the saturated vapour pressure versus air temperature curve is

$$e(T)=0.6108\exp\left(\frac{17.27T}{T+237.3}\right), \quad (A.2)$$

where T denotes the daily air temperature, and e_s of the day can be calculated by

$$e_s=\frac{e(T_{\max})+e(T_{\min})}{2}, \quad (A.3)$$

where $T_{\max}$ and $T_{\min}$ are maximum and minimum daily air temperatures, respectively.

The GCM outputs are daily $T_{\max}$, $T_{\min}$ (which can be used to calculate e_s and Δ), u_2 and RH. Assuming G equals 0 and if we compute R_n, we can use Equation (A.1) to estimate E_p. The process of utilizing the solar radiation (R_s) to compute R_n is described below.

Firstly, we calculate the incoming net short wave radiation (R_{ns}) by

$$R_{ns}=(1-\alpha)R_s, \quad (A.4)$$

where α denotes the albedo.

Next, the net outgoing long-wave radiation (R_{nl}) is estimated by

$$R_{nl}=\sigma\left(\frac{T_{\max}^4+T_{\min}^4}{2}\right)\left(0.34-0.14\sqrt{e_a}\right)\left(1.35\frac{R_s}{R_{s0}}-0.35\right), \quad (A.5)$$

where σ is the Stefan–Boltzmann constant (=4.903×10^{-9} MJ K^{-4} m^{-2} day^{-1}), e_a is the actual vapour pressure (=$e_s \times$ RH), and R_{s0} is the clear-sky solar radiation, which can be computed by

$$R_{s0}=(0.75+2\times10^{-5}z)R_a, \quad (A.6)$$

where z is the station elevation above sea level (m), which is available from the GCMs, and R_a is the extraterrestrial radiation (MJ m^{-2} d^{-1}) determined by Equations (21) to (25) in Allen et al. (1998).

Finally, by subtracting R_{nl} from R_{ns}, we obtain R_n.

Appendix B

This appendix provides an explicit description of the derivation of the framework for estimating k_Q and $\Delta\overline{Q}$ from Equation (8). Substituting Equation (8) into Equation (2) yields

$$k_Q = \frac{\sum_{i=1}^{m}(t_i-\bar{t})(\varepsilon_P \Delta P_i + \varepsilon_0 \Delta E_{\mathrm{p}i})}{\sum_{i=1}^{m}(t_i-\bar{t})^2}. \quad \text{(B.1)}$$

This equation can be transformed into

$$k_Q = \varepsilon_P \frac{\sum_{i=1}^{m}(t_i-\bar{t})\Delta P_i}{\sum_{i=1}^{m}(t_i-\bar{t})^2} + \varepsilon_0 \frac{\sum_{i=1}^{m}(t_i-\bar{t})\Delta E_{\mathrm{p}i}}{\sum_{i=1}^{m}(t_i-\bar{t})^2}. \quad \text{(B.2)}$$

Recalling the definition of the trend in this study, Equation (B.2) can be considered a linear combination of k_P and $k_{E_{\mathrm{p}}}$:

$$k_Q = \varepsilon_P k_P + \varepsilon_0 k_{E_{\mathrm{p}}}.$$

Equation (3) can be rewritten as

$$\Delta\overline{Q} = \frac{\sum_{i=1}^{m} Q_{\mathrm{p}i} - m\bar{Q}}{m}. \quad \text{(B.3)}$$

Recombination of the variables leads to the following expression:

$$\Delta\overline{Q} = \frac{\sum_{i=1}^{m}(Q_{\mathrm{p}i} - \bar{Q})}{m}. \quad \text{(B.4)}$$

Similarly, the substitution of Equation (8) yields

$$\Delta\overline{Q} = \frac{\sum_{i=1}^{m}(\varepsilon_P \Delta P_i + \varepsilon_0 \Delta E_{\mathrm{p}i})}{m}. \quad \text{(B.5)}$$

We finally obtain the target equation:

$$\Delta\overline{Q} = \varepsilon_P \Delta\overline{P} + \varepsilon_0 \Delta\overline{E_{\mathrm{p}}}.$$

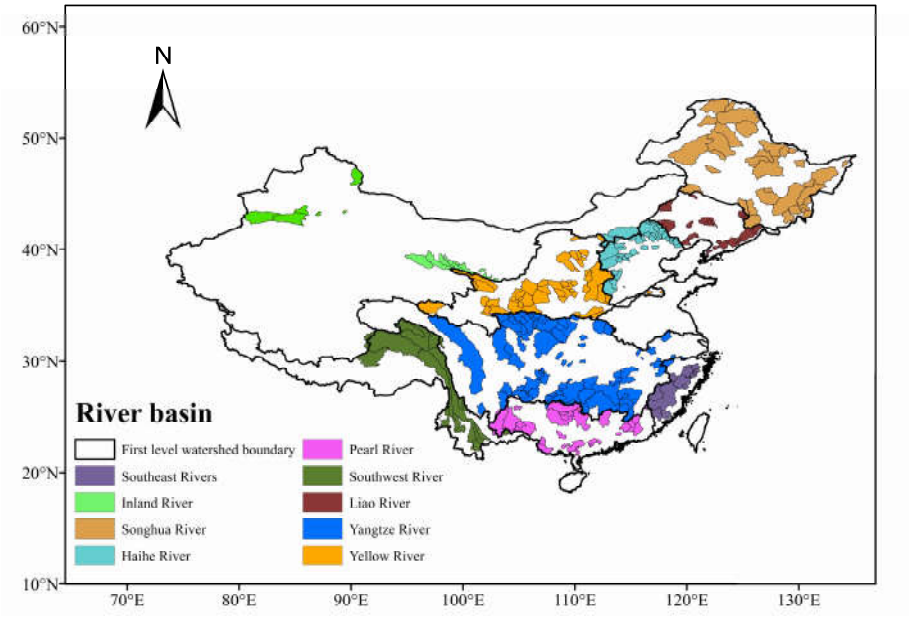

Figure 1: Spatial distribution of the 291 study catchments across mainland China.

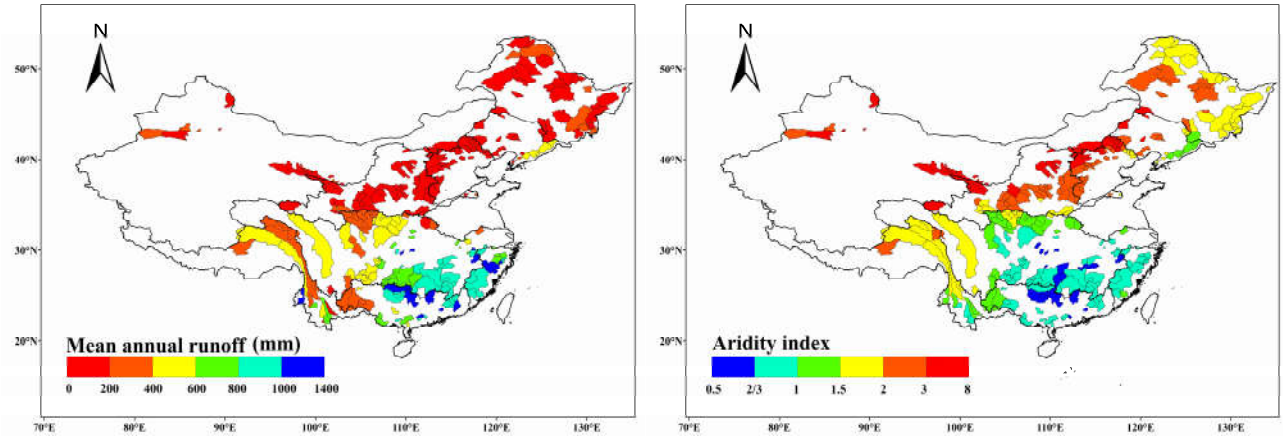

Figure 2: Spatial distribution of mean annual runoff $\overline{Q}$ (left) and aridity index φ (right) in the 291 study catchments.

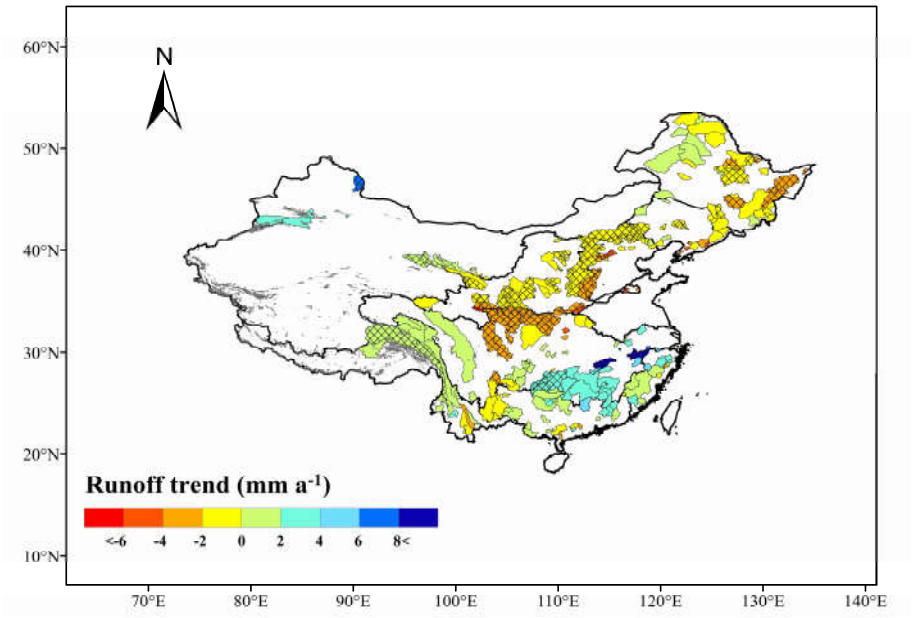

Figure 3: The observed runoff trends (k_Q) in the 291 catchments for the period of 1956 to 2000. Dark red and blue denote catchments with a trend smaller than -6 mm a^{-1} and larger than 8 mm a^{-1}, respectively. Crosshatched areas are significant catchments (p7). Grey shaded areas are glaciers based on the second glacier inventory data set of China (Guo et al., 2014).

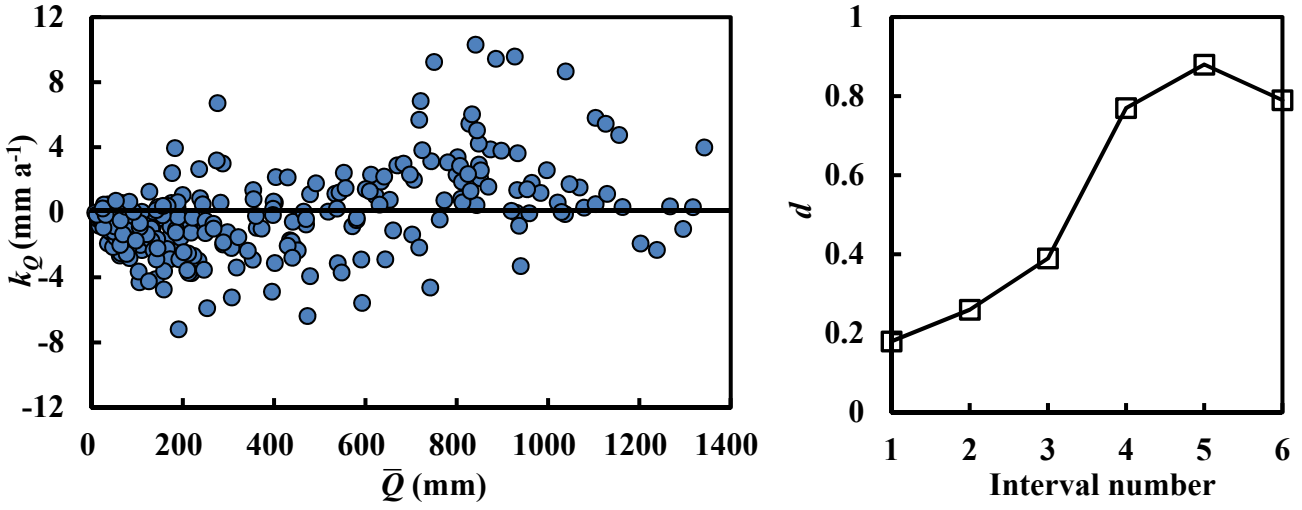

Figure 4: Relationship between observed runoff trends k_Q and mean annual runoff $\overline{Q}$ for the study catchments (left) and values of *d* in each interval according to $\overline{Q}$ (right). *d* denotes the proportion of catchments with positive trends in each interval. Interval numbers 1 to 6 correspond to six intervals 0–200, 200–400, 400–600, 600–800,800–1000 and 1000–1400.

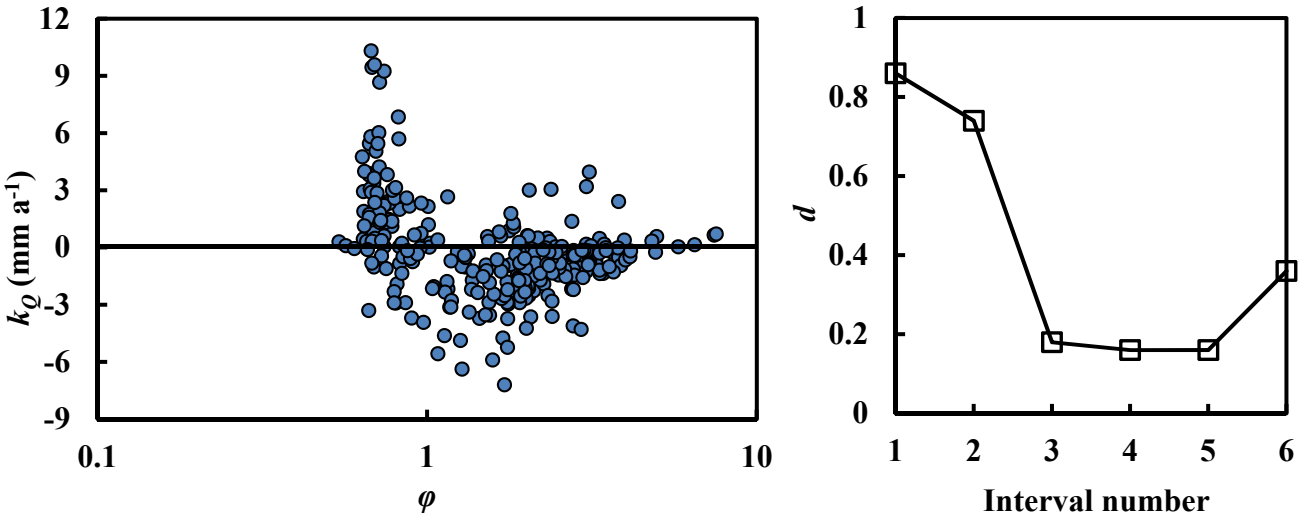

Figure 5: Relationship between observed runoff trends k_Q and mean annual runoff $\overline{Q}$ for the study catchments (left) and values of d in each interval according to φ (right). Interval numbers 1 to 6 correspond to six intervals 0.5–2/3, 2/3–1, 1–1.5, 1.5–2,2–3 and 3–8.

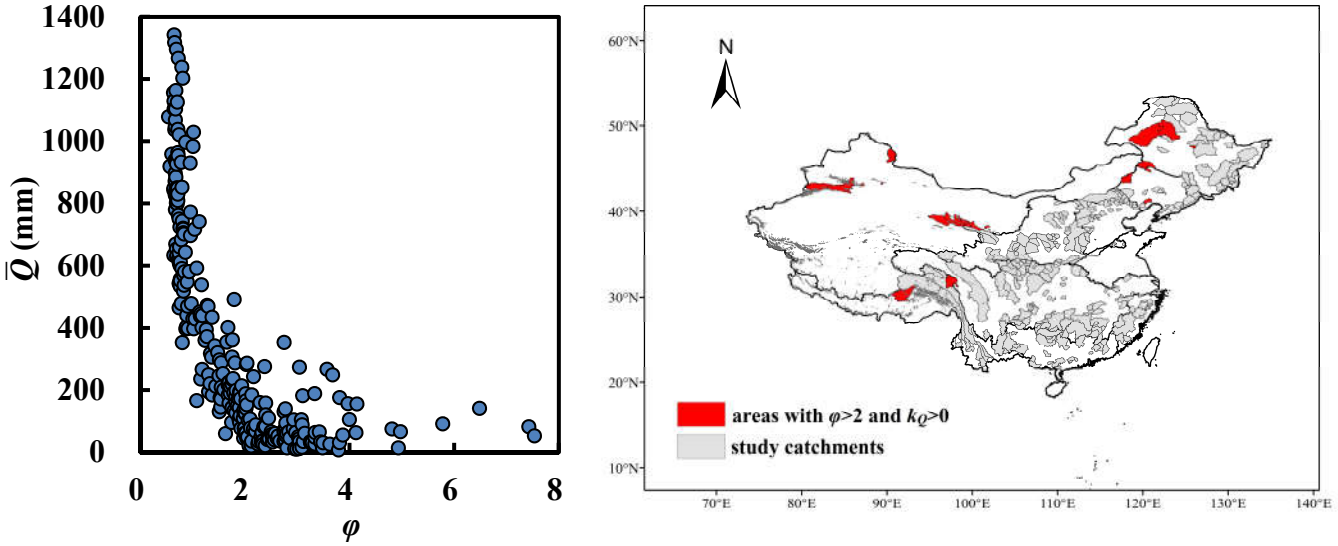

Figure 6: Relationship between mean annual runoff $\overline{Q}$ and aridity index φ in the study catchments (left) and the distribution of catchments with φ>2 and k_Q>0 (right). Grey shaded areas are glaciers based on the second glacier inventory data set of China (Guo et al., 2014).

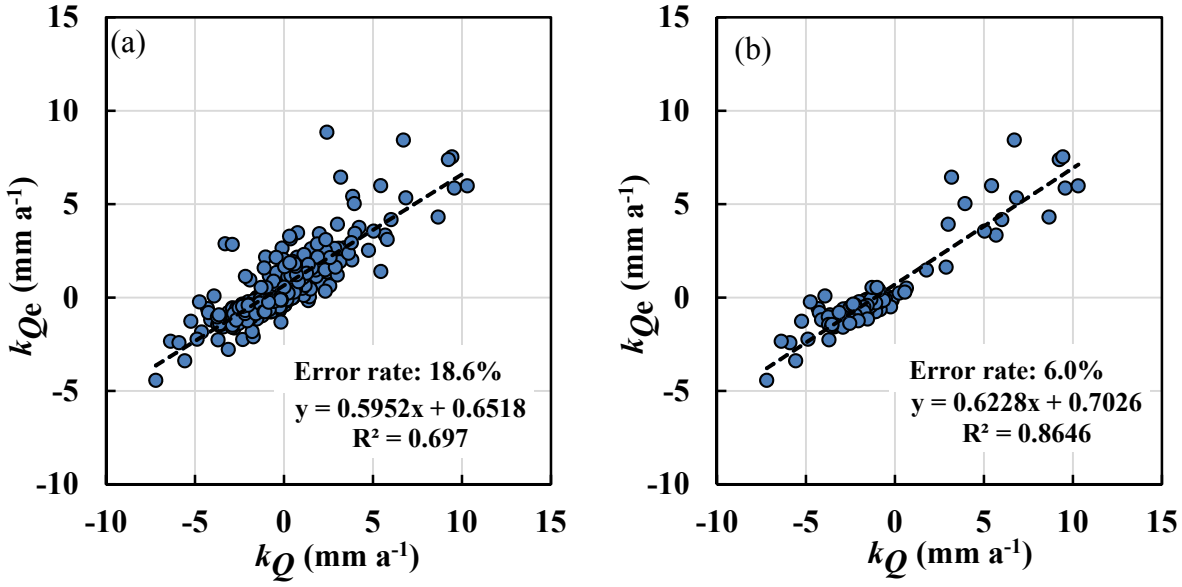

Figure 7: Comparison of estimated runoff trends k_{Qe} with observed trends k_Q for (left) all catchments and (right) significant catchments. Significant catchments are ones experiencing significant changes in runoff at the significance level of 0.05. The error rate is defined as the proportion of catchments in which the signs of the observed and estimated trends differ.

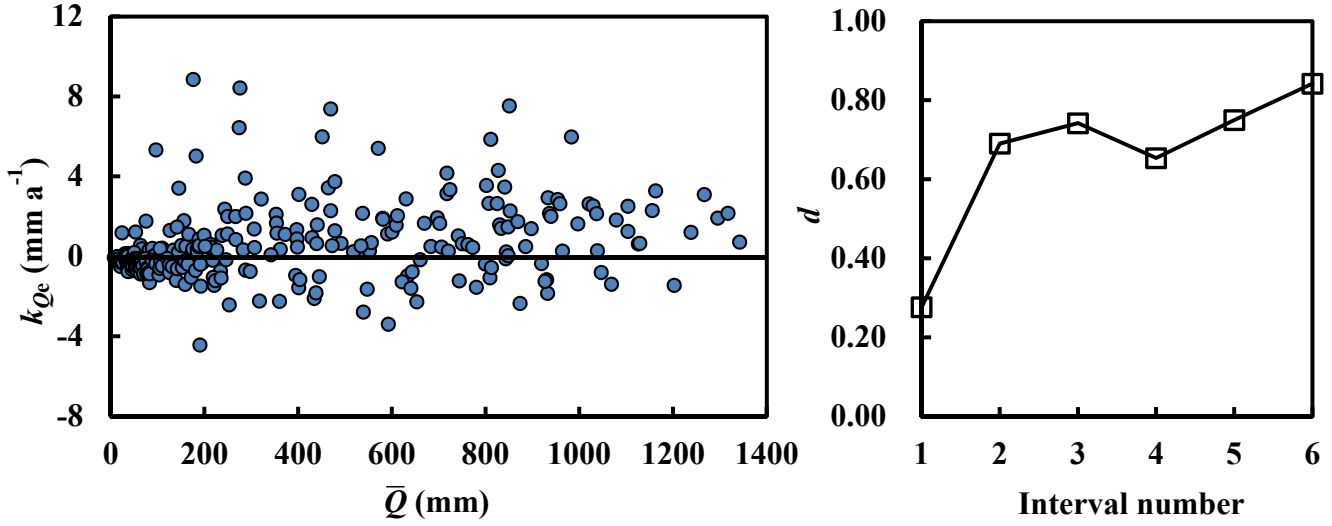

Figure 8: Relationship between observed runoff trends k_{Qe} and mean annual runoff $\overline{Q}$ for the study catchments (left) and values of d in each interval according to $\overline{Q}$ (right). Interval numbers 1 to 6 correspond to six intervals 0–200, 200–400, 400–600, 600–800,800–1000 and 1000–1400.

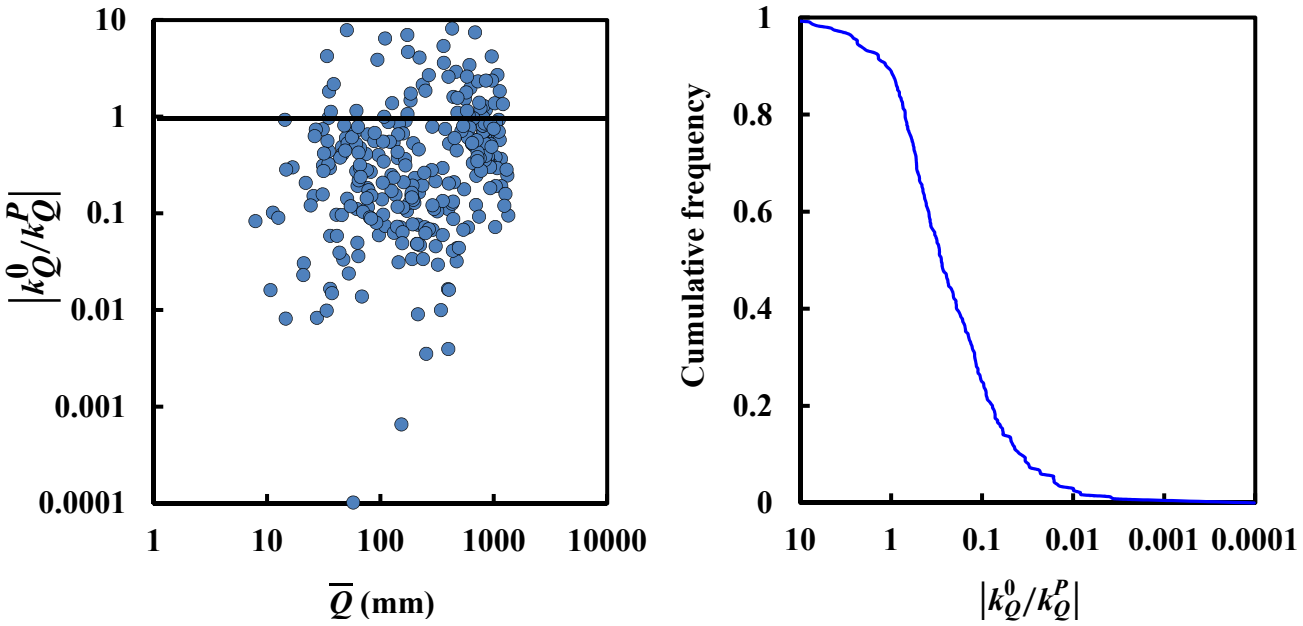

Figure 9: Exploring the controlling factor in the DDWW pattern according to the Budyko hypothesis. (left) Relationship between the ratio of absolute k_Q^0 (=$\varepsilon_0 k_{E_p}$, the part of the estimated runoff trends k_{Qe} generated from potential evapotranspiration changes**)** to absolute k_Q^P (= $\varepsilon_P k_P$, the part of k_{Qe} generated from precipitation changes) and the mean annual runoff $\overline{Q}$. **(right)** The cumulative frequency curve of $\left|k_Q^0/k_Q^P\right|$.

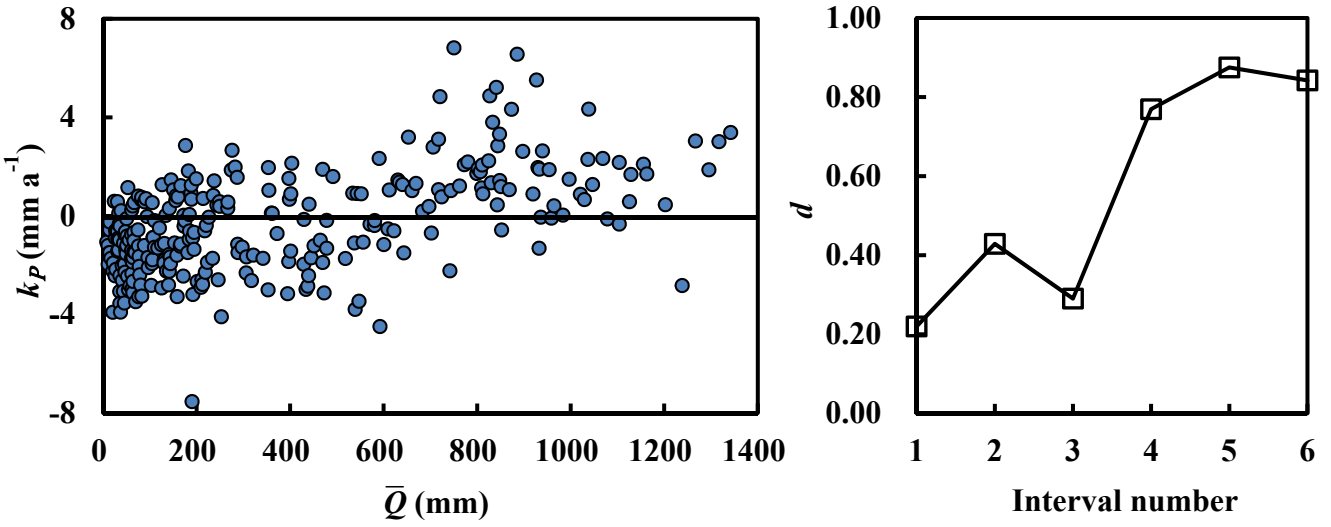

Figure 10: Relationship between observed runoff trends k_P and mean annual runoff $\overline{Q}$ for the study catchments (left) and values of d in each interval according to $\overline{Q}$ (right). Interval numbers 1 to 6 correspond to six intervals 0–200, 200–400, 400–600, 600–800,800–1000 and 1000–1400.

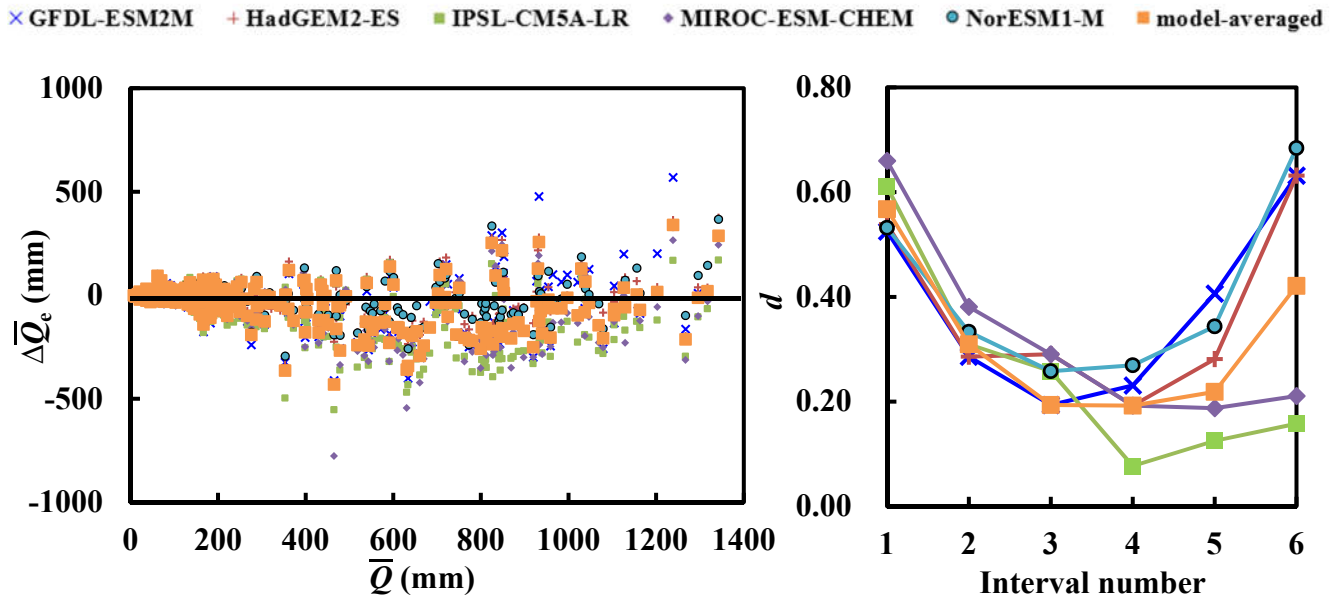

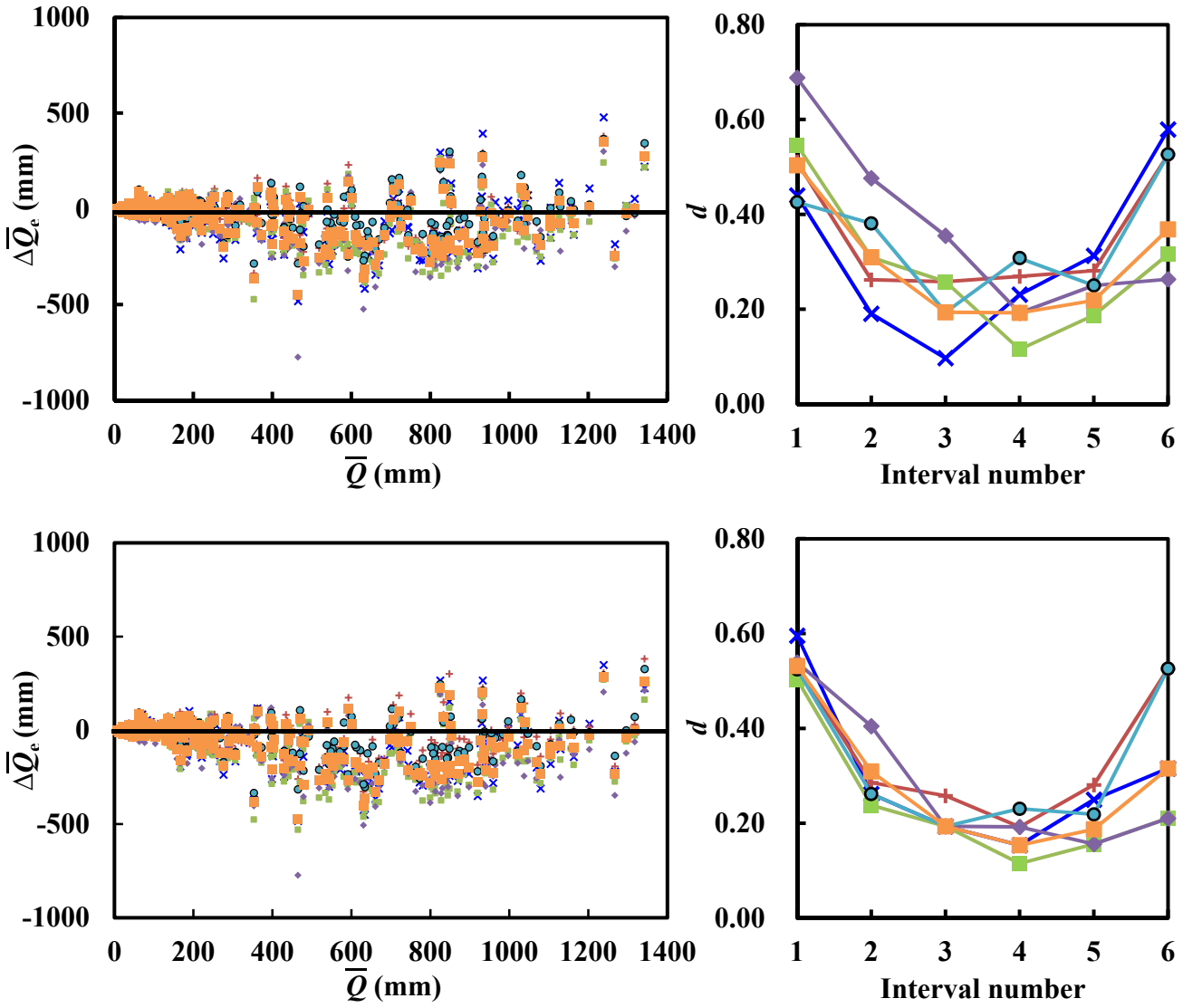

Figure 11: Projections of future trends $\Delta\overline{Q}_e$ under (top) RCP2.6, (middle) RCP4.5 and (bottom) RCP8.5 scenarios for the period 2001-2050. (left column) Relationship between projected $\Delta\overline{Q}_e$ of the five models and their means and mean annual runoff $\overline{Q}$. **(right column)** Values of d in each interval according to $\overline{Q}$ based on $\Delta\overline{Q}_e$ of the five models and their means. Interval numbers 1 to 6 correspond to six intervals 0–200, 200–400, 400–600, 600–800,800–1000 and 1000–1400.

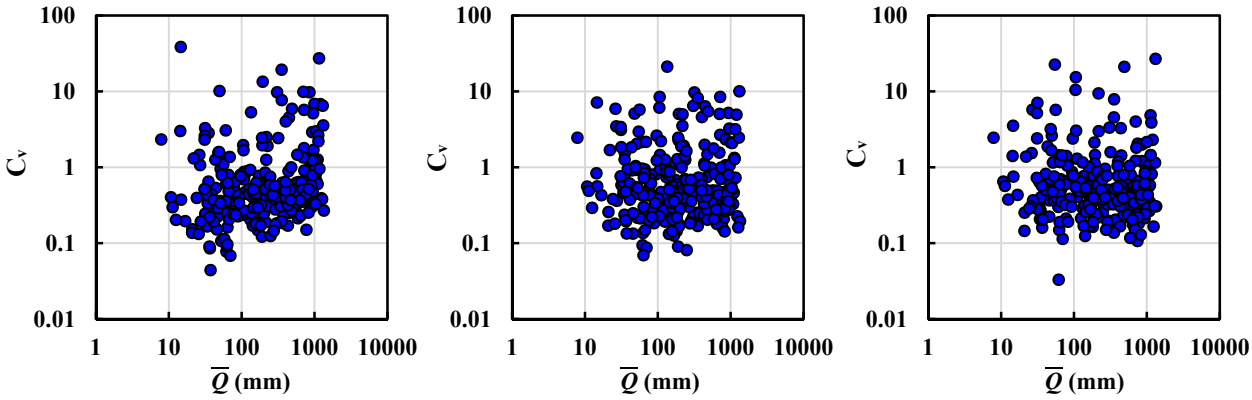

Figure 12: C_v values of projected future trends $\Delta\overline{Q}_e$ under (left) RCP2.6, (middle) RCP4.5 and (right) RCP8.5 Scenarios.

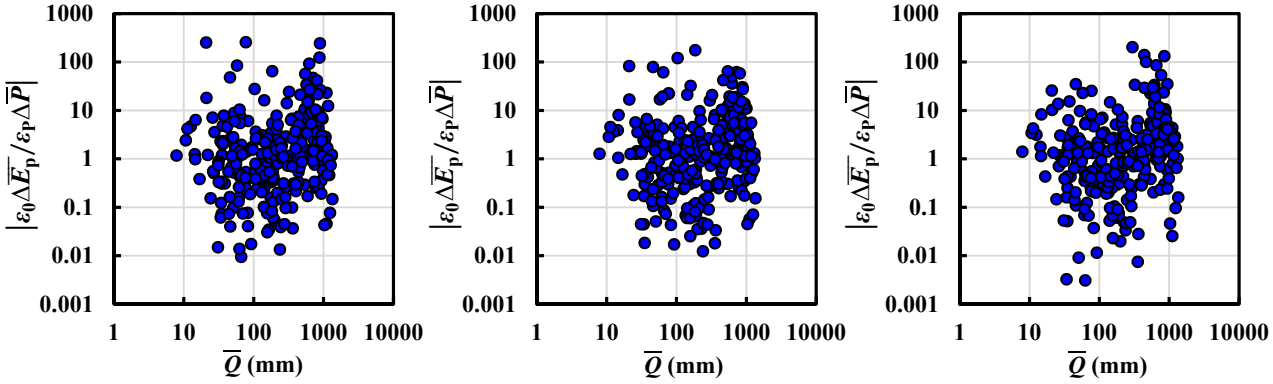

5

Figure 13: Exploring the controlling factor in the projected climate change under (left) RCP2.6, (middle) RCP4.5 and (right) RCP8.5.

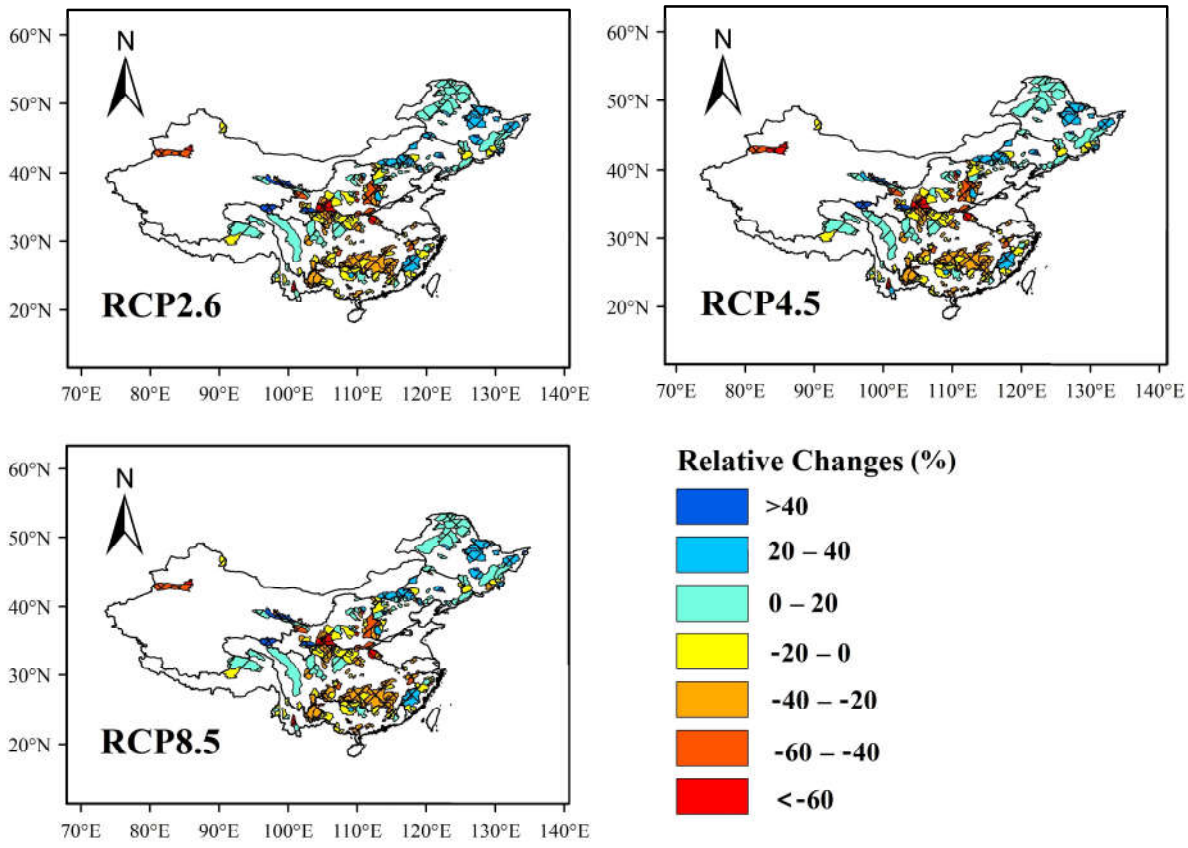

Figure 14: Spatial distribution of the model-averaged relative changes in mean annual runoff $\overline{Q}$ (=$\Delta\overline{Q}_e/\overline{Q}$) for the period of 2001 to 2050 under three different scenarios. Hatched areas denote regions with C_v values smaller than 0.5, whereas double-hatched areas represent regions with C_v values smaller than 1.

5

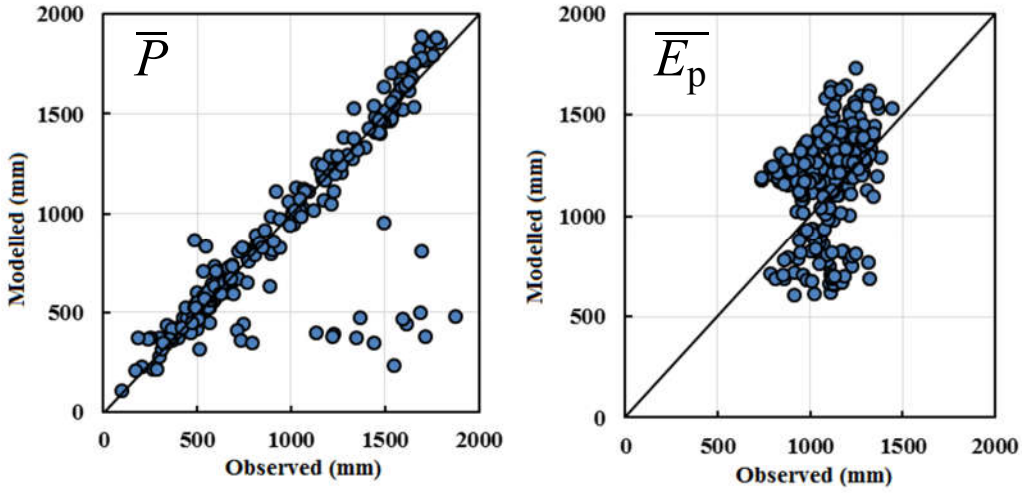

Figure 15: Comparison of the observed meteorological data with the simulations from the GFDL-ESM2M model for the period 1956–2000.

Table 1: Details of the interval partitions based on mean annual runoff $\overline{Q}$ and aridity index φ.

Interval number	Interval range	Sample size
Based on $\overline{Q}$		
1	0-200	141
2	200-400	42
3	400-600	31
4	600-800	26
5	800-1000	32
6	1000-1400	19
Based on φ		
1	0.5-2/3	21
2	2/3-1	72
3	1-1.5	33
4	1.5-2	55
5	2-3	68
6	3-8	42

Table 2: Number of catchments with k_Q>0 and respective d in each interval based on $\overline{Q}$ and φ in the analysis of the observed trends.

Interval number	Number of catchments with k_Q>0	d
Based on $\overline{Q}$		
1	26	0.18
2	11	0.26
3	12	0.39
4	20	0.77
5	28	0.88
6	15	0.79
Based on φ		
1	18	0.86
2	53	0.74
3	6	0.18
4	9	0.16
5	11	0.16
6	15	0.36

Table 3: Numbers of catchments with $\Delta\overline{Q}_e>0$ and respective *d* in each interval based on $\overline{Q}$ of five GCMs and their means in the analysis of the projected trends under three scenarios.

	Interval number	1	2	3	4	5	6
RCP2.6							
GFDL-ESM2M	Number	74	12	6	6	13	12
	d	0.52	0.29	0.19	0.23	0.41	0.63
HadGEM2-ES	Number	76	12	9	5	9	12
	d	0.54	0.29	0.29	0.19	0.28	0.63
IPSL-CM5A-LR	Number	86	13	8	2	4	3
	d	0.61	0.31	0.26	0.08	0.13	0.16
MIROC-ESM-CHEM	Number	93	16	9	5	6	4
	d	0.66	0.38	0.29	0.19	0.19	0.21
NorESM1-M	Number	75	14	8	7	11	13
	d	0.53	0.33	0.26	0.27	0.34	0.68
Model-averaged	Number	80	13	6	5	7	8
	d	0.57	0.31	0.19	0.19	0.22	0.42
RCP4.5							
GFDL-ESM2M	Number	62	8	3	6	10	11
	d	0.44	0.19	0.10	0.23	0.31	0.58
HadGEM2-ES	Number	72	11	8	7	9	10
	d	0.51	0.26	0.26	0.27	0.28	0.53
IPSL-CM5A-LR	Number	77	13	8	3	6	6
	d	0.55	0.31	0.26	0.12	0.19	0.32
MIROC-ESM-CHEM	Number	97	20	11	5	8	5
	d	0.69	0.48	0.35	0.19	0.25	0.26
NorESM1-M	Number	60	16	6	8	8	10
	d	0.43	0.38	0.19	0.31	0.25	0.53
Model-averaged	Number	71	13	6	5	7	7
	d	0.50	0.31	0.19	0.19	0.22	0.37
RCP8.5							
GFDL-ESM2M	Number	84	11	6	4	8	6

	d	0.60	0.26	0.19	0.15	0.25	0.32
HadGEM2-ES	Number	75	12	8	5	9	10
	d	0.53	0.29	0.26	0.19	0.28	0.53
IPSL-CM5A-LR	Number	71	10	6	3	5	4
	d	0.50	0.24	0.19	0.12	0.16	0.21
MIROC-ESM-CHEM	Number	76	17	6	5	5	4
	d	0.54	0.40	0.19	0.19	0.16	0.21
NorESM1-M	Number	74	11	6	6	7	10
	d	0.52	0.26	0.19	0.23	0.22	0.53
Model-averaged	Number	75	13	6	4	6	6
	d	0.53	0.31	0.19	0.15	0.19	0.32